



Novel Synthesis and Characterization of Nano-Activated Carbon Derived from Agricultural Orange Peel Waste



Enas Sameer Alkhawaja^{1,2*}, Hayder Mohammed Abdul-Hameed¹

¹ Department of Environmental Engineering, College of Engineering, Baghdad University, Baghdad 10071, Iraq

² AL Najaf Health Department, Ministry of Health Iraq, Najaf 54001, Iraq

Corresponding Author Email: inas.abd2111p@coeng.uobaghdad.edu.iq

Copyright: ©2025 The authors. This article is published by IETA and is licensed under the CC BY 4.0 license (<http://creativecommons.org/licenses/by/4.0/>).

<https://doi.org/10.18280/ijdne.200104>

ABSTRACT

Received: 1 November 2024

Revised: 29 November 2024

Accepted: 6 December 2024

Available online: 31 January 2025

Keywords:

activated carbon, agricultural waste, activation, carbonization, orange peels, nanomaterials

Orange peel, often discarded as waste, is a common byproduct of agricultural and food processing industries. Converting this waste into valuable materials reduces environmental pollution and promotes circular economy practices. The increasing recognition of orange peels may be attributed to their ease of obtaining from agricultural products. Here, we synthesize activated carbon from orange peels by carbonizing orange peel powder with N₂ gas and activating it with CO₂ gas. Characterization of synthesis activated carbon from orange peel OP-AC done by using FTIR, TEM, EDS, Raman spectroscopy, SEM, and BET. The specific surface area (SBET) of the activated carbon (AC) and orange peel (OP) are 7.9168 m²/g and 3.879 m²/g, respectively. Also, the total pore volume for AC and OP are 0.027785 cm³/g and 0.01789 cm³/g, respectively. Orange peel-activated carbon (OP-AC) exhibits a turbostratic structure and lamellar morphology, with the presence of inorganic impurities, and is primarily composed of micropores. In summary, the synthesis of nanostructured activated carbon from orange peel waste is a promising innovation with potential applications in environmental remediation, energy storage, wastewater and water treatment and industrial processes. It contributes to sustainability by turning agricultural waste into a high-value material, supporting both environmental and economic benefits.

1. INTRODUCTION

Citrus is the second largest growing fruit in the world, The citrus production is estimated at 80 million tonnes per year making it an important source for useful to human health components [1]. Orange peel, often discarded as waste, is a common byproduct of agricultural and food processing industries. Converting this waste into valuable materials (such as activated carbon) helps reduce environmental pollution and promotes circular economy practices. With its affordable and superior qualities, activated carbon is a powder material that may be used in wide range of adsorption applications. Numerous documented sources of AC have been mentioned, such as petroleum pitch, rose husk, fly ash, coal, lignite, and coconut shell. The increasing recognition of orange peels as a resource is due to their widespread availability as a byproduct of agriculture and food processing [2]. The fruit's peel is the main waste during the manufacturing of orange juice, while the remaining 50% (w/w) comprises peel, pulp, seeds, and membranes [3]. Therefore, turning orange peels, a relatively inexpensive agricultural waste, into usable materials like adsorbents might increase the residue's value and help with the biomass disposal issue [4]. Samples of orange peel content from Iraq percentages of carbohydrates, fat, protein, ash, and moisture, respectively, are 19.24, 0.21, 5.50, 4.25, and 70.50 [5]. Activated carbon is one well-known material employed in

a variety of environmental applications, particularly for the purification of wastewater and water. Aqueous systems may effectively remove both organic and inorganic pollutants from water systems because of activated carbon materials' large surface area, microporous arrangement, and a high degree of surface reactivity [6]. Activated carbon from tea and coffee waste from the pyrolysis process continued to be burnt in the furnace to expand the surface area of the adsorbent and improve adsorption capacity and efficiency [7]. A collection of amorphous carbonaceous powder possessing a well-developed internal pore structure and a highly crystalline form is collectively referred to as activated carbon. After undergoing carbonization and activation of its natural source's constituents, almost any organic substance can be employed as the precursor or starting material for activated carbon [8].

The process described in this study involves two steps: the first is chemical activation using N₂, and the second is physical or thermal activation using CO₂. These two steps are then implemented. physical activation is chosen due to being less expensive [9]. In this study, activated carbon is synthesized from orange peels through carbonization under N₂ gas and activation with CO₂ gas. Characterization of synthesized activated carbon from orange peel (OP-AC) is conducted using FTIR, excessive-resolution TEM (HRTEM), strength dispersive spectroscopy (EDS), Raman spectroscopy, scanning electronic microscopy (SEM). The specific surface

area (SBET) of AC and OP are calculated using the BET method, with values of 7.9168 m²/g and 3.879 m²/g, respectively. Also, the total pore volume for AC and OP is 0.027785 cm³/g and 0.01789 cm³/g, respectively, determined at P/P₀ = 0.99 from N₂ single point adsorption and the useful organizations to locate FTIR were used to explain OP-AC. OP-AC exhibits a turbostratic structure and lamellar morphology, with the presence of inorganic impurities, and is primarily composed of micropores. In summary, synthesis of nanostructured carbon from orange peel waste is a promising innovation with potential applications in environmental remediation, energy storage, wastewater and water treatment, and industrial processes. It contributes to sustainability by turning agricultural waste into a high-value material, supporting both environmental and economic benefits. This can reduce waste management costs while providing economic benefits in various industries. Nano-activated carbon (OP-AC) derived from organic waste like orange peel is an environmentally friendly and sustainable alternative to traditional carbon sources, reducing the reliance on fossil fuels and non-renewable resources.

2. MATERIALS AND METHODS

2.1 Synthesis and production of activated carbon

Orange peels (OP) from Iraq were used as raw materials. Orange peel is an inexpensive, readily and abundantly available agricultural byproduct of the orange juicing business. OP's chemical makeup consists of limonene, chlorophyll pigments, lignin, pectin, hemicellulose and cellulose [10]. Through the carbonization-activation process, the activated carbon AC-OP was created. Orange peel was washed with tap water, allowed to dry in the sun for a few days or until they are entirely dry, and then ground into a powder using a machine grinder to prepare orange peel powder (OP) and the particle size of the powdered orange peel was controlled by sieve analysis after grinder. Afterwards, the powdered carbon that is activated was obtained by passing N₂ gas at a flowing rate of 0.5 L/min for duration of 1 hour in a furnace with a temperature of 200°C, followed by a passage of CO₂ gas at a flowing rate of 0.5 L/min for duration of 1 hour in a furnace with a temperature of 250°C both of them with heating rate optimized at (35°C/min) which is the controlled loop of rising temperature of the furnace to reach the adjusted on the rate. Switch off the CO₂ flow to obtain activated carbon (AC-OP) and then store it in sealed glass containers. The samples were carbonized and activated using a furnace (Model: 62700, 1488 Watts, 220-240 Volts, 6.2 Amps), manufactured in Japan. The reason for choosing a 200°C and 250°C burning degree in a furnace done by repeated burning runs with different degree and chosen the best one that give a black gray activated carbon. Figure 1 shows the general synthesis procedure for the preparation material.



(a) Dry orange peel



(b) Powder (Crushed) of orange peel



(c) Carbonization with N₂ gas and Activation with CO₂ gas



(d) Activated carbon sourced from orange peel

Figure 1. An overall process for producing activated carbon from orange peel

3. CHARACTERIZATION OF ACTIVATED CARBON

In general, material characterization needs to be appropriate for its intended use, meaning that the method selected for characterization ought to consider the type of data needed for the specific application of the material being examined.

As was previously indicated, the ultimate product and the source of the activated carbon should both be taken into consideration when characterizing material obtained from lignocellulosic sources. Analyzing the raw material to ascertain its purity, primary chemical structure, particle shape, and size. Important details regarding the characteristics of the finished product can be found in the proximate analysis carried out before the carbonization phase and the ultimate analysis carried out afterward [11-14].

The sample's morphology was examined using a transmission electron microscope (TEM) equipped with a Philips model CM120 and a scanning electron microscope (SEM) equipped with a Jasco 4200 Japan instrument for FTIR testing. Measurements using energy dispersive spectroscopy (EDS) were done at Oxford Instruments, UK. Using a Raman thermos nickel Raman spectrometer from the USA, Raman spectroscopy was performed. Powders were subjected to analysis in an X-ray diffraction apparatus with a Siemens model D500 detector. Test (BET) for Brunare and Eimattauer conducted by Quanta Chrome NOVA 2200E in Germany.

3.1 XRD test

The X-ray diffraction of OP and AC was used to evaluate the crystalline form. A crystalline is composed of regularly arranged in a 3D zone. In contrast, amorphous materials have an unregular arrangement and atoms are randomly distributed

in the 3D zone [15]. The best calcination temperature is 250°C; it was checked with crystal phase, weight loss and surface area [16]. running with CuK α radiation at 45 kV and 25 mA. At a scan speed of 0.42° s⁻¹, within the 2 θ range, which extends from 10° to 90°, XRD patterns were obtained. The diffractograms displayed in Figure 2 lack a sharp peak and have broad peaks instead. The powdered orange peel's amorphous nature can be indicated by the lack of a distinct peak. In contrast, a large peak in Figure 3 (between 2 θ from (28.4822 to 29.0547) indicated the beginnings of a crystalline carbonaceous structure, which improved layer alignment [17].

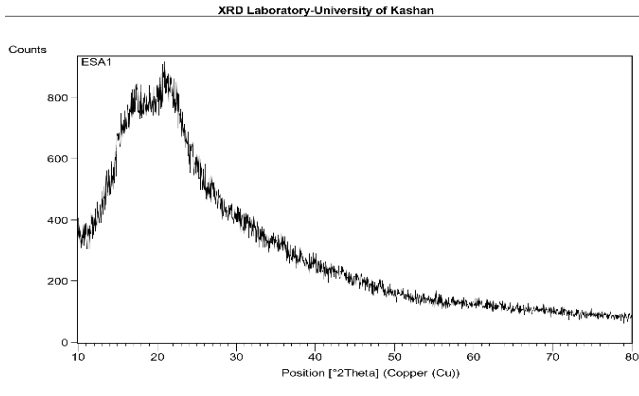


Figure 2. XRD test of raw powder orange peel

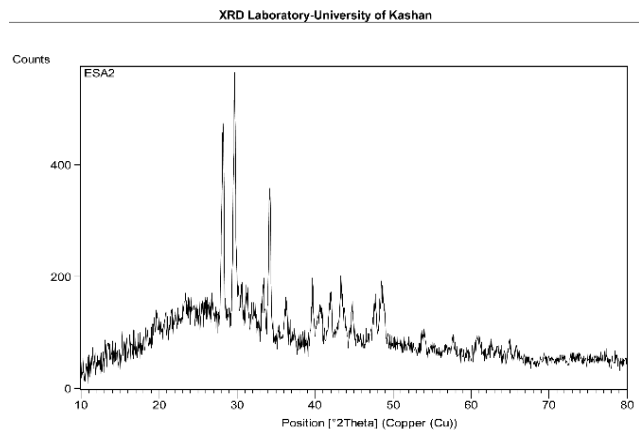


Figure 3. XRD test of activated carbon of orange peel

The crystal structure of the produced activated carbon was analyzed using an X-ray diffractometer. The diffraction patterns of carbon derived from orange peel are indicated by the following planes: (002) at 13.4°, (101) at 19.5°, (111) at 29.4°, (020) at 34.1°, and (022) at 39.4°, as illustrated in Figure 3 [18]. Additionally, there are extra peaks present, which may be attributed to the presence of pure biomass and the graphitic structure of carbon [12, 13, 19, 20].

XRD measurements described the structures of the synthesized OP and OP-AC samples, the results of which are displayed in Figure 2 and Figure 3. The OP samples show a wide Peak, which refers to poor crystallization, as confirmed by the XRD findings. The two large peaks at 24.24° and 43.01° are attributed to the reflection from the carbon's (002) and (101) planes. The massive peaks at 24.24 result from the amorphous nature of the carbon molecules and diffusion scattering of the degree of graphitization [21].

It was observed that in OP-AC, the (002) peak's intensity is noticeably lower, but its widening is higher. It indicates that

the samples have a high density of pores. Furthermore, the interlayer spacing is calculated using Bragg's equation, which states that $2d \sin \theta = n\lambda$. For the FG sample, the crystallite size is 25.84 nm, as calculated below. The observed d spacing of the AC-OP is larger than the OP graphite results [22].

3.1.1 Crystallite size

The crystallite size and average crystallite size were calculated from XRD data. The crystallite size, D, was calculated using Scherrer's equation, and the results are presented in Table 1.

$$D = \frac{K\lambda}{\beta_{hkl} \cos \vartheta_{hkl}} \quad (1)$$

where,

D = size in (nm)

K = 0.95-0.98 (shape factor)

λ = 0.154 nm (X-ray wavelength)

β_{hkl} = half-width of the diffraction band (FWHM) (radians)

ϑ_{hkl} = Bragg diffraction angle (peak position in radians)

Table 1. Value of the above equation obtained by using origin lab soft

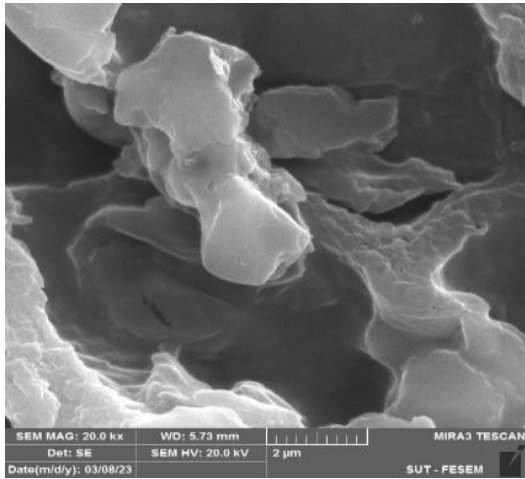
Peak Position (2 θ)	FWHM (β)	Size (D) (nm)
23.092	0.64361	13.29298617
24.3704	0.53993	15.88275597
25.35246	0.39312	21.8553921
26.5217	0.40144	21.45278105
28.10368	0.38615	22.37715967
29.44079	0.37061	23.3853407
34.04951	0.48543	18.05932201
36.06166	0.42095	20.94141958
37.91918	0.49134	18.03887396
39.50223	0.4292	20.75101903
43.23828	0.70708	12.75197097
47.43494	0.6401	14.30348323
48.55939	0.55053	16.70344007
49.17176	0.08972	102.7429506
53.92806	1.13465	8.288679438
69.42139	0.25325	40.26481756
21.17387	1.20322	7.087261235
13.61344	0.73116	11.54586428
12.00968	0.75566	11.15398441
10.43028	0.45385	18.54625168
17.15634	0.43113	19.66275748
15.09797	0.95146	8.887035222
30.59667	0.06138	141.5821609
30.59667	0.57338	15.15628909
44.8243	0.42572	21.29866269

Average size= 25.84 nm.

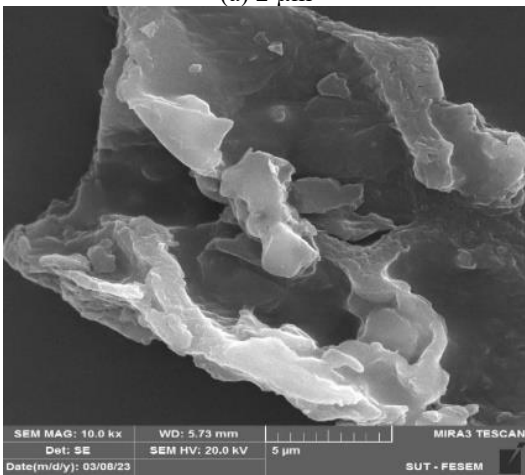
3.2 SEM test characterization

Observed the morphology powder of orange peel and activated carbon from orange peel by using scanning electron microscope (SEM). The SEM images at Figure 4(a, b and c) for orange peel show at scale of (a) 2 μ and (b) 5 μ m and (c) 500nm an irregular surface morphology. The surface of activated carbon materials in Figure 5(a, b, and c), shown at scales of 2 μ m, 10 μ m, and 500 nm, is characterized by a well-developed structure, as evidenced by the presence of holes with various diameters and shapes, including irregularly shaped holes. The existence of a porous structure facilitates the diffusion process indispensable in heterogeneous catalysis for the transport of both reactants and products [23]. This coarse

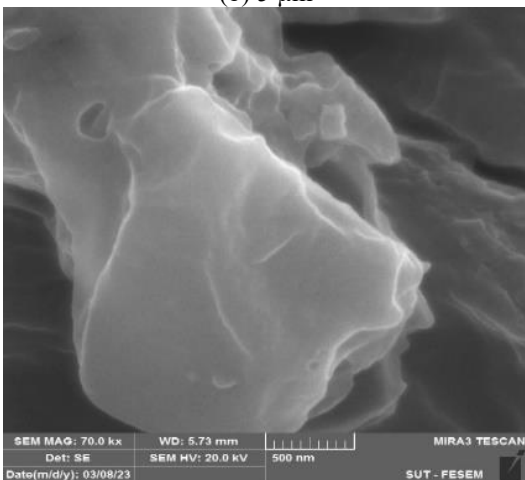
texture comprises varying-sized pores, making it useful for adsorption purposes [24].



(a) 2 μ m



(b) 5 μ m



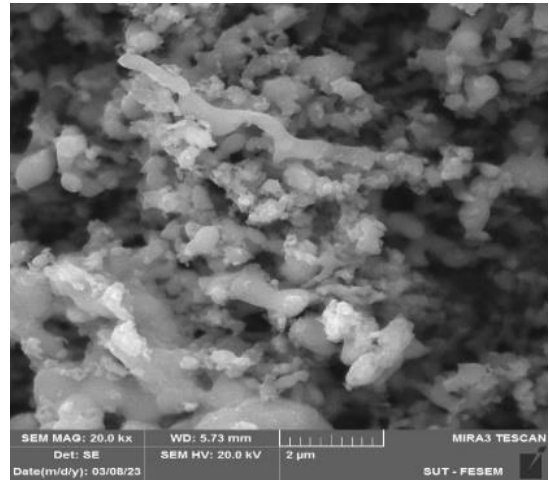
(c) 500 nm

Figure 4. SEM test of powder orange peel (a) at a scale of 2 μ , (b) at a scale of 5 μ , and (c) at a 500nm scale

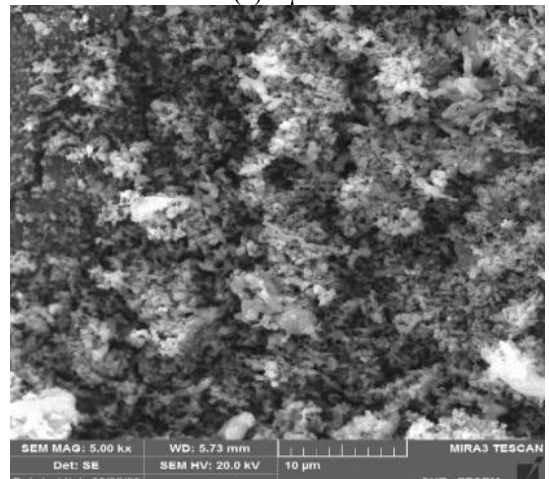
The porous channel in the OP structures was visible in the scanning electron microscope (SEM) micrographs shown in Figure 5, resulting from the pyrolysis and chemical activation of carbon produced from the orange peel precursor. The pre-carbonized precursor was pyrolyzed without a chemical activation agent to create a structure with asymmetric morphologies, as shown in Figure 5(b). Studies [25, 26] show carbon develops in a porous condition when a channel

assembly is visible. This gives electrolyte ions access a greater surface area and a transfer pathway along the charge storage progression.

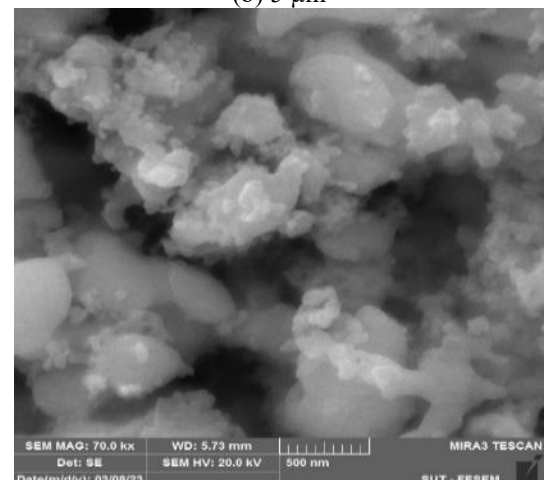
SEM imaging reveals the surface morphology and pore distribution of a material. A high surface area, often associated with a porous structure, is critical for enhancing adsorption capacity. Greater surface area provides more active sites for adsorption, enabling the material to capture larger amounts of adsorbates.



(a) 2 μ m



(b) 5 μ m



(c) 500 nm

Figure 5. SEM test of activated carbon a) at the scale of 2 μ , (b) at the scale of 5 μ , and (c) at a 500nm scale

3.3 Energy dispersive spectroscopy (EDS) test characteristic

a schema of the particle content of activated carbon are carbon (C), Oxygen (O), potassium (K), calcium (Ca), Magnesium (Mg), phosphorus (P), sulfur (S), and chlorine (Cl). The majority of these components are said to be a feature of the makeup of orange peels by studies [27, 28]. Table 3 shows that the concentrations of K (8.65%) and Ca (6.87%) are significantly greater than those of the other elements, yet they are nevertheless regarded as typical for Iraqi oranges. Oxygen's presence indicates that the activated carbon has a high content of oxygen-containing functional groups.

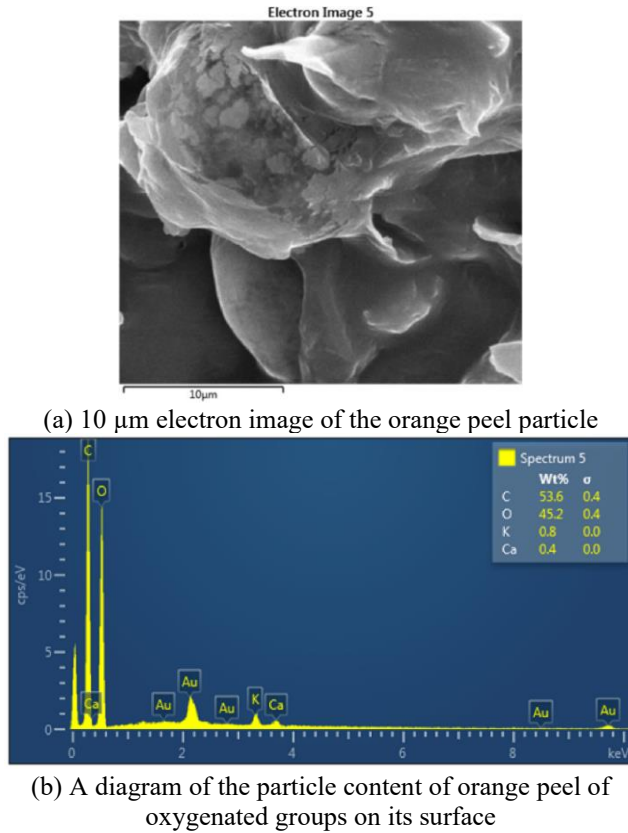


Figure 6. EDS test of orange peel

Using energy dispersive spectroscopy (EDS) to find the orange peel sample's and activated carbon's chemical composition. The test reports are displayed in Figure 6(a), 10μm electron schema of the orange peel particle. A diagram of the particle content of orange peel is shown in Figure 6(b) and Table 2. These diagrams and table show that the OP is constituted of some elements, such as, carbon (C), Oxygen (O), potassium (K) and calcium (Ca).

While for activated carbon, Figure 7 shows the following results: (a) a 10 μm electron image of the activated carbon, (b)

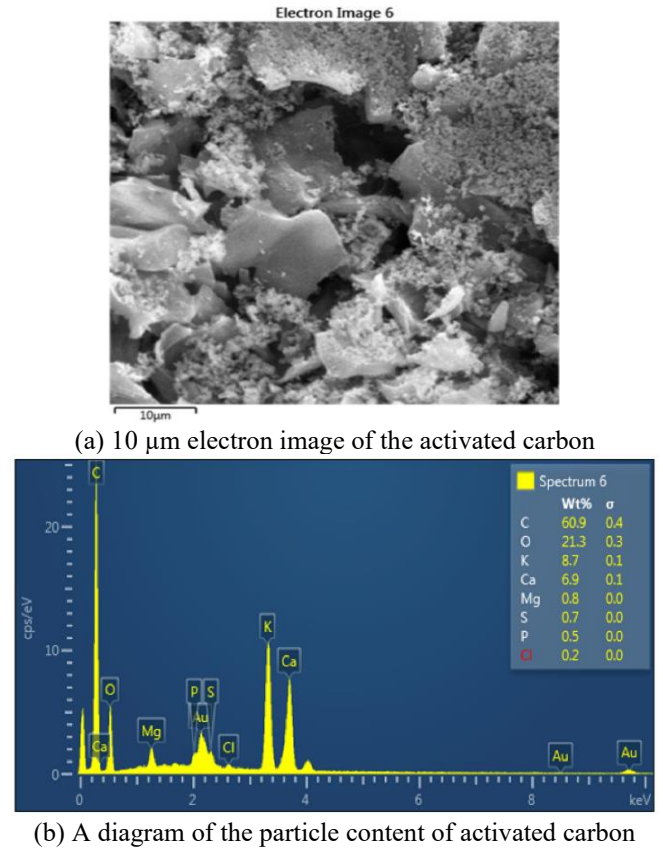


Figure 7. EDS test of activated carbon

Table 2. EDS test of the particle content of orange peel

Element	Line Type	Apparent Concentration	k Ratio	Wt%	Wt% Sigma	Atomic %
C	K series	9.24	0.09238	53.61	0.39	60.98
O	K series	9.49	0.03193	45.21	0.39	38.61
K	K series	0.33	0.00279	0.77	0.04	0.27
Ca	K series	0.17	0.00149	0.40	0.04	0.14
Total				100		100

Table 3. EDS test of the particle content of the particle content of activated carbon from orange peel

Element	Line Type	Apparent Concentration	k Ratio	Wt%	Wt% Sigma	Atomic %
C	K series	12.71	0.12706	60.87	0.37	73.73
O	K series	3.61	0.01214	21.34	0.35	19.41
Mg	K series	0.38	0.00253	0.82	0.04	0.49
P	K series	0.45	0.00249	0.55	0.04	0.26
S	K series	0.37	0.00322	0.71	0.04	0.32
Cl	K series	0.10	0.00086	0.19	0.03	0.08
K	K series	4.90	0.04150	8.65	0.10	3.22
Ca	K series	3.61	0.03223	6.87	0.09	2.49
Total				100		100

3.4 FTIR test

There is a clear structural similarity when comparing the wavelength of the orange peel (OP) from the graph in Figure 8 with the data in Table 4. The bands of the hydroxyl groups of proteins and carbohydrates are visible at 3422.06 cm^{-1} , while the C-H stretching vibrations of aliphatic groups are observed at 2919.7 cm^{-1} . At 2346.94 cm^{-1} , certain weak bands

are linked to C=C conjugated and C=C bonds, depending on the vegetable origin of the samples. The bands at 1750 cm^{-1} correspond to the C=O group, and a strong peak appears at 1637.27 cm^{-1} , corresponding to the C=O amide I group. At 1457.92 cm^{-1} , stretching -C=O, inorganic carbonate is found at the peak. the protein structures' amide III band at (1327.75 cm^{-1}), as well as the C-X of fluoride at (1057.76 cm^{-1}) and chloride at (669.178 cm^{-1}).

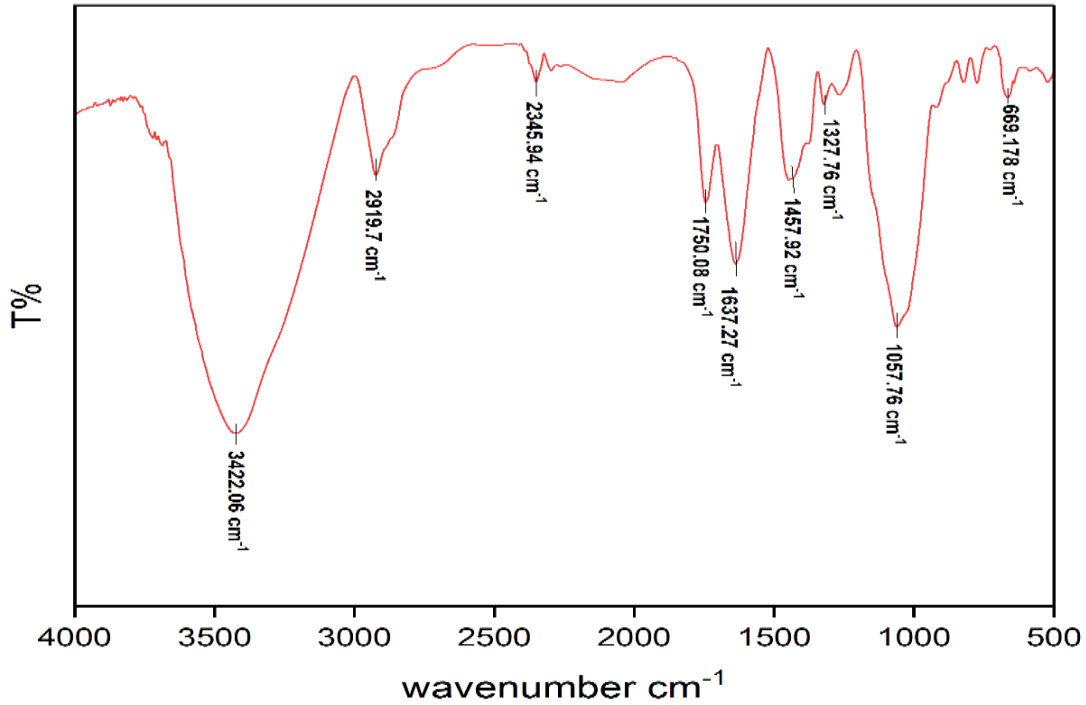


Figure 8. Test of powder orange peel

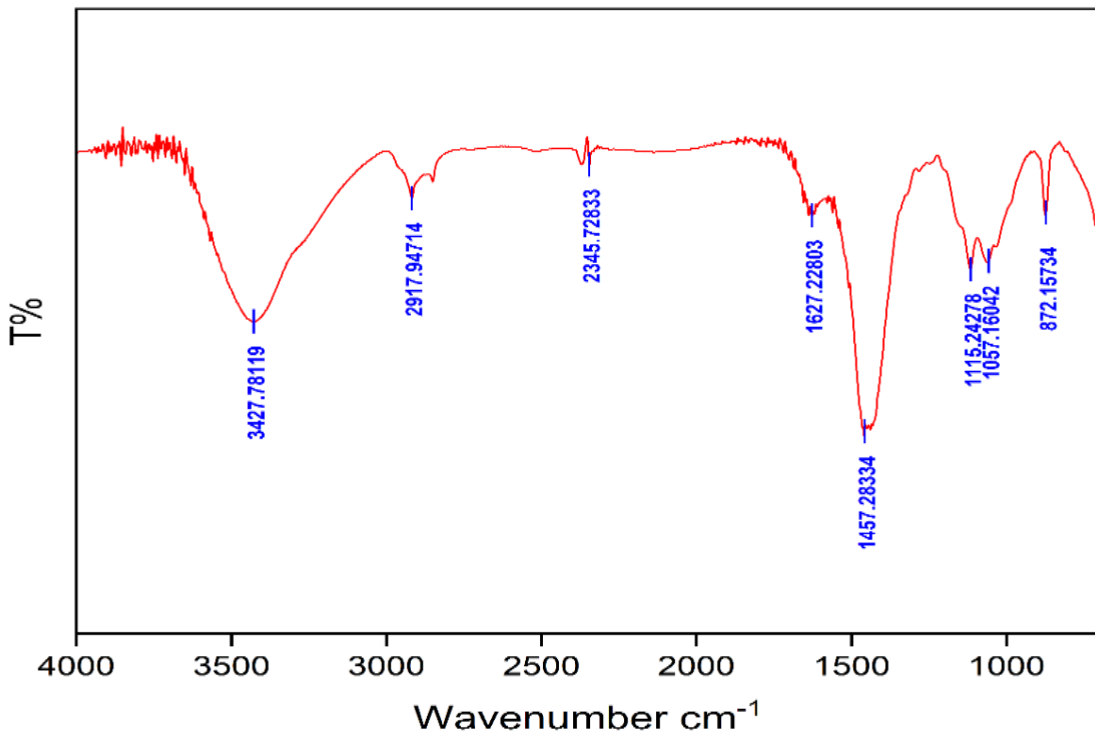


Figure 9. FTIR test of activated carbon from orange peel

Figure 9 depicts the AC absorption spectrum. The stretching of the O-H group is connected to the peaks at (3427.78 cm^{-1}). On the other hand, the (2917.94 cm^{-1}) peak is caused by the C-H stretching [29]. The additional peaks at (2345.94 cm^{-1}) and (1627.22 cm^{-1}) are connected to C=C functional groups (1457.28 cm^{-1}) are connected to C=O functional groups. The peak at (1057.16 cm^{-1}) is attributed to the C-O deformation of the aromatic group of graphitic units. These peaks demonstrate the presence of hydrophilic functional groups on the activated carbon's surface [30].

The presence or absence of functional groups in the OP and AC-OP samples was determined using FTIR spectroscopy; the results are displayed in Figures 8 and 9. The majority of the functional groups are present in the FTIR spectra of OP and AC-OP. In contrast to OP, AC-OP exhibits lower-intensity absorbance peaks following the activation process. As a result, the various functional groups present in OP and AC-OP may give rise to pores.

Table 4. List of band assignments for FTIR

Wavenumber cm^{-1}	Functional Group
3350-3450	O-H
2850-3000	C-H
2100-2500	C=C conjugated and C=C
1690-1760	Stretching C=O
1600-1680	C=C
1400-1460	Stretching C=O inorganic carbonate
1050-1250	C-O-C stretch
1000-1450	C-O
600-900	C-H out of the plane

3.5 TEM studies

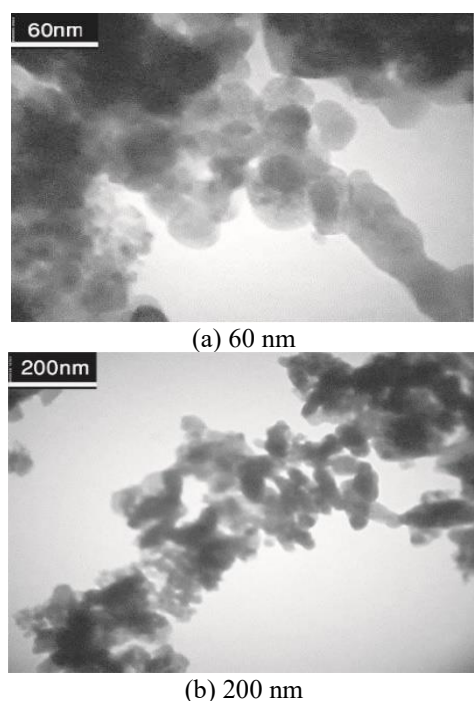


Figure 10. TEM test of orange peel (a) at scale of 200 nm and (b) at scale of 60 nm

TEM measurements were used to analyze the synthetic materials' structural morphologies. Figure 10 displays the OP powder's TEM image pattern results. Figure 11 depicts the porous and densely linked frameworks with the crystallinity of AC-OP. This kind of AC-OP texture morphology suggests that

the pores that are created during the carbonization and activation process help with ion diffusion within the carbon texture [31].

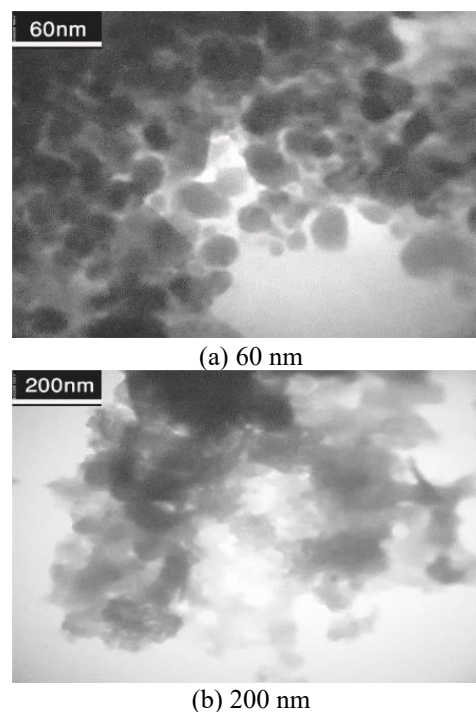


Figure 11. TEM test of activated carbon orange peel (a) at a scale of 200 nm and (b) at a scale of 60 nm

3.6 Raman spectrum

High-quality graphene can be quickly identified by Raman spectroscopy. Figure 12 and Figure 13 show the Raman spectroscopy graph of orange peel (OP) and activated carbon sourced from orange peel (OP-AC) respectively, these diagrams show a multi narrow peaks the high centered at (415.21 and 317.39) cm^{-1} for OP and (1533.23 and 1580.7) cm^{-1} for OP-AC. These peaks are ascribed to the intensity of the 2D band relative to the G band (I_{2D}/I_G) = $2908.29/1589.74=1.829$ greater than > 0.5 which means a purity measure. Additionally, Their peaks at $\sim 2914.98\text{ cm}^{-1}$ and $\sim 3045.24\text{ cm}^{-1}$, respectively, emphasize the turbostratic nature of FG.

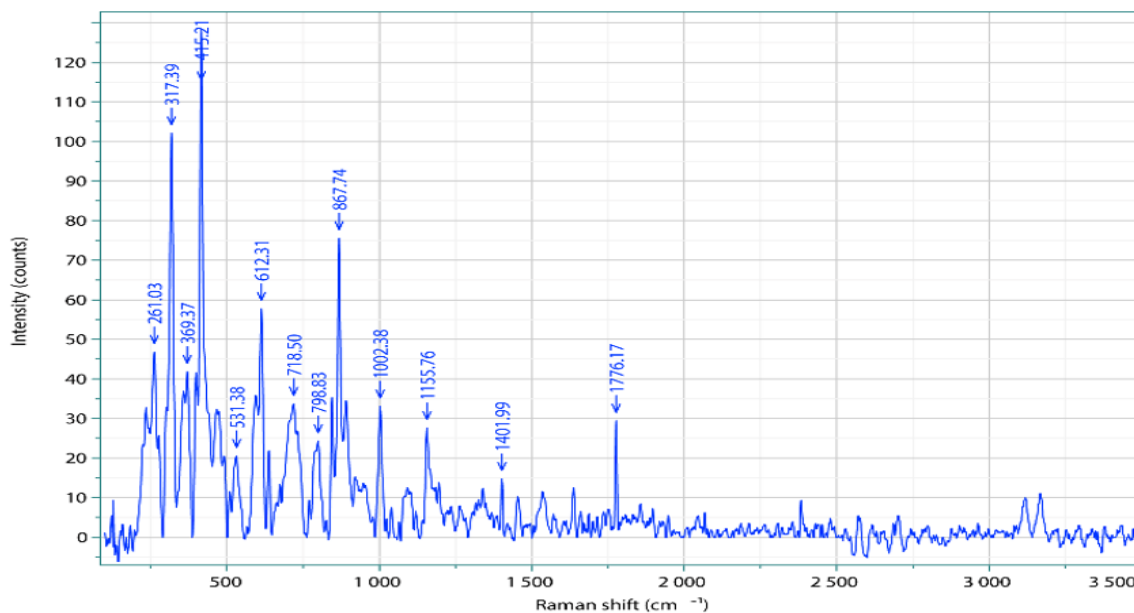
3.7 BET analysis

The physicochemical properties of the AC and OP surfaces, including total pore volume, mean pore diameter, and specific surface area, were determined using BET surface area analysis. The pore structure properties are presented in Table 5. The BET test refers to the Brunauer–Emmett–Teller (BET) analysis, which is a widely used method for determining the specific surface area of a material. This test is based on the adsorption of gas molecules (commonly nitrogen, N_2) onto the surface of a material at a constant temperature (typically 77 K, the boiling point of liquid nitrogen). The specific surface areas (SBET) of AC and OP were calculated using the BET method [30], yielding values of $7.9168\text{ m}^2/\text{g}$ and $3.879\text{ m}^2/\text{g}$, respectively. The BJH method [23] was applied to analyze the pore size and volume.

The total pore volumes of AC and OP were determined to be $0.027785\text{ cm}^3/\text{g}$ and $0.01789\text{ cm}^3/\text{g}$, respectively, at $P/P_0 =$

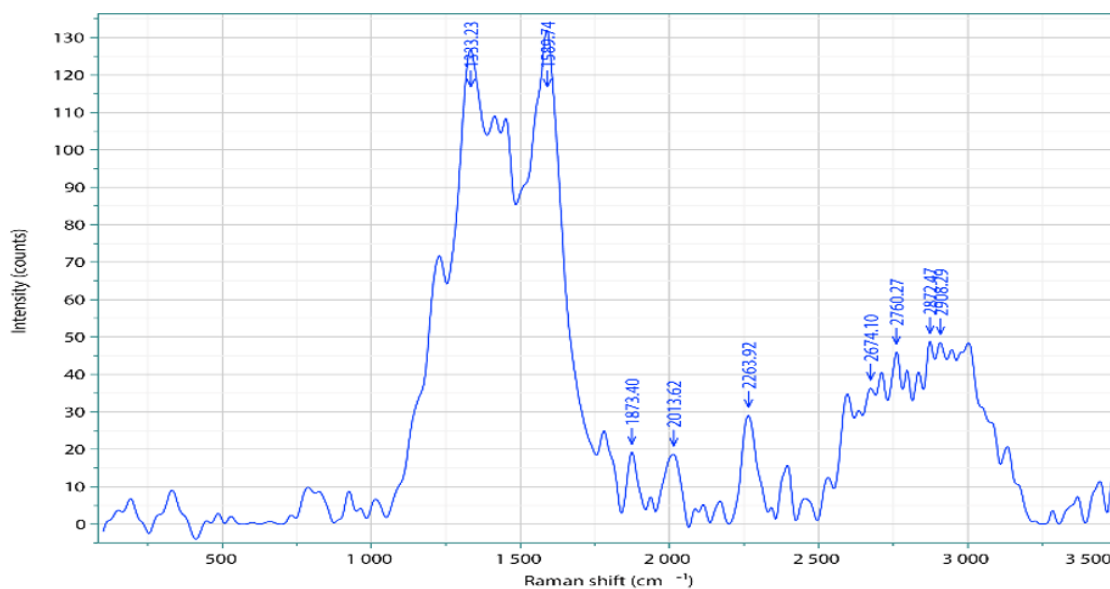
0.99 from N₂ single-point adsorption. The mean pore widths of AC and OP were 14.039 nm and 18.448 nm, respectively. These values indicate the mesoporous nature of the materials, as porous materials are classified as microporous (less than 2

nm), mesoporous (between 2 and 50 nm), or microporous (greater than 50 nm) [32, 33]. The surface area and pore volume of macropores, mesopores, and micropores can be determined using BJH, the t-plot approach, and BET [34].



Date	11.03.2023	Acq. time (s)	8	Accumulations	4	Laser	785 nm Edge
Spectro (cm⁻¹)	300	Hole (µm)	300	Slit (µm)	100	Grating	1200 (750nm)
Filter	25%	Objective	x100_VIS	ICS correction	Off	Range (cm⁻¹)	0 – 3500

Figure 12. Raman spectroscopy test of powder orange peel



Date	11.03.2023	Acq. time (s)	4	Accumulations	2	Laser	785 nm Edge
Spectro (cm⁻¹)	300	Hole (µm)	300	Slit (µm)	100	Grating	1200 (750nm)
Filter	10%	Objective	x100_VIS	ICS correction	Off	Range (cm⁻¹)	0 – 3500

Figure 13. Raman spectroscopy test of activated Carbone from orange peel

In adsorption applications, the BET surface area and pore size distribution are fundamental parameters that determine the efficiency and capacity of the adsorbent. A higher BET surface area provides more adsorption sites, while an appropriate pore size distribution ensures that adsorbates can efficiently access these sites. This leads to better performance in various applications such as gas storage, water treatment,

and catalysis. Understanding and optimizing both properties is essential for designing advanced materials tailored to specific adsorption processes.

Surface area is crucial in determining the active sites available for contaminant adsorption. Increasing the surface area of a material enhances its ability to adsorb a larger quantity of pollutants [35]. The N₂ adsorption-desorption

isotherms were used to measure the specific surface area and porous structure of the prepared activated carbon. Techniques such as BET and BJH were employed to calculate the surface area of the prepared activated carbon [36]. The surface area (BET) and porosity are key indicators of optimal preparation conditions. As shown in Figure 9, the volume adsorbed increases with increasing relative pressure. The SBET and total pore volume (VT) of the prepared activated carbon are

influenced by the type of agricultural waste used. The carbonization and activation processes improved the adsorption capacity and efficiency by increasing the surface area of the adsorbent. For comparison, the physical properties of tea waste before and after activation show that the surface area increased from 0.735 m²/g (before activation) to 72.857 m²/g (after activation), similar increased in the surface area as the results obtained in study [37].

Table 5. Textural characteristics of AC and OP

Samples	SBE m ² /g	dp nm (2t)	V _T cm ³ /g	Average Pore Diameter (nm)	V _{BJH} cm ³ /g	V, meso cm ³ /g	a _p m ² /g
OP	3.879	24.616	0.01789	18.448	0.020221	0.8912	8.7738
AC	7.9168	3.0995	0.027785	14.039	0.027705	1.8189	7.3368

4. CONCLUSION

In conclusion, easily available discarded orange peel has been utilized as a predecessor to make AC-OP porous frameworks. The TEM data indicates that the three-dimensional porous structures with pores are apparent in the AC-OP. FTIR and Raman investigations verify that the AC-OP has defects and different functional groups.

To sum up, orange peels, a biomass precursor, were successfully converted into activated carbons using both chemical and physical activation. The prepared materials' amorphous structure was confirmed by XRD analysis, and the carbonaceous materials that were obtained exhibited a well-developed surface. SEM spectroscopy of the examined samples showed a high degree of purity and an uneven surface shape, with the carbon materials' surface showing signs of inorganic matter content.

The recommended method of generating activated carbons from waste biomass and the way in which these carbons are employed for the development of activated carbon is an effective way to transform natural resources into materials and compounds with a wide variety of applications and because of it has a high surface area, which makes it highly effective in adsorbing pollutants, heavy metals, and toxins from water and air. It can be applied in water treatment, air purification, gas adsorption and waste management to remove contaminants. Nano activated carbon's smaller particle size enhances its reactivity and adsorption efficiency, making it a more efficient material for environmental cleanup processes compared to conventional activated carbon. These raw materials are abundant, inexpensive, and renewable. It just takes two gasses to produce the activated carbons in this easy-to-follow method. As a result, this process is inexpensive and produces little chemical waste.

REFERENCES

[1] Abass, E.H., Zair, S.K., Mohammud, T.K., Nagem, S.A. (2014). Recovery of pure Hesperidin from Iraqi Sweet Oranges Peel and study the effect in some bacteria. *Baghdad Science Journal*, 11(2): 455-460. <https://doi.org/10.21123/bsj.2014.11.2.455-460>

[2] Kosheleva, R.I., Mitropoulos, A.C., Kyzas, G.Z. (2019). Synthesis of activated carbon from food waste. *Environmental Chemistry Letters*, 17: 429-438. <https://doi.org/10.1007/s10311-018-0817-5>

[3] de Moraes Barros, H.R., de Castro Ferreira, T.A.P.,

Genovese, M.I. (2012). Antioxidant capacity and mineral content of pulp and peel from commercial cultivars of citrus from Brazil. *Food Chemistry*, 134(4): 1892-1898. <https://doi.org/10.1016/j.foodchem.2012.03.090>

[4] Rodrigues, L.A., da Silva, M.L.C.P., Alvarez-Mendes, M.O., dos Reis Coutinho, A., Thim, G.P. (2011). Phenol removal from aqueous solution by activated carbon produced from avocado kernel seeds. *Chemical Engineering Journal*, 174(1): 49-57. <https://doi.org/10.1016/j.cej.2011.08.027>

[5] Liu, Q.S., Zheng, T., Wang, P., Jiang, J.P., Li, N. (2010). Adsorption isotherm, kinetic and mechanism studies of some substituted phenols on activated carbon fibers. *Chemical engineering journal*, 157(2-3): 348-356. <https://doi.org/10.1016/j.cej.2009.11.013>

[6] Ruiz, B., Ferrera-Lorenzo, N., Fuente, E. (2017). Valorisation of lignocellulosic wastes from the candied chestnut industry. Sustainable activated carbons for environmental applications. *Journal of Environmental Chemical Engineering*, 5(2): 1504-1515. <https://doi.org/10.1016/j.jece.2017.02.028>

[7] Abd AL-Hussain, Z.K., Hameed, H.M.A. (2022). Study for the production of local adsorbent from tea and coffee wastes for removal of lead ions from an aqueous solution. *International Journal of Health Sciences*, 6(S6): 6947-6955. <https://doi.org/10.53730/ijhs.v6nS6.11957>

[8] Bansal, R.C., Goyal, M. (2005). *Activated Carbon Adsorption*. CRC Press. <https://doi.org/10.1201/9781420028812>

[9] Abdullah, S.R., Razaq, R.K.A. (2018). Extracting carotenoids pigments from citrus peel and studying their functional properties. *Tikrit Journal for Agricultural Sciences*, 18(4): 146-163.

[10] Naser, Z.A., Abdul-Hameed, H.M. (2022). Removal of Cu (II) from industrial wastewaters through locally-produced adsorbent prepared from orange peel. *Caspian Journal of Environmental Sciences*, 20(1): 45-53. <https://doi.org/10.22124/CJES.2022.5391>

[11] Fu, K., Yue, Q., Gao, B., Sun, Y., Zhu, L. (2013). Preparation, characterization and application of lignin-based activated carbon from black liquor lignin by steam activation. *Chemical Engineering Journal*, 228: 1074-1082. <https://doi.org/10.1016/j.cej.2013.05.028>

[12] González, P.G., Pliego-Cuervo, Y.B. (2013). Physicochemical and microtextural characterization of activated carbons produced from water steam activation of three bamboo species. *Journal of Analytical and Applied Pyrolysis*, 99: 32-39.

- <https://doi.org/10.1016/j.jaap.2012.11.004>
- [13] Kumar, A., Jena, H.M. (2016). Preparation and characterization of high surface area activated carbon from Fox nut (*Euryale ferox*) shell by chemical activation with H₃PO₄. *Results in Physics*, 6: 651-658. <https://doi.org/10.1016/j.rinp.2016.09.012>
- [14] Wilkins, C.K., Clausen, P.A., Wolkoff, P., Larsen, S.T., et al. (2001). Formation of strong airway irritants in mixtures of isoprene/ozone and isoprene/ozone/nitrogen dioxide. *Environmental Health Perspectives*, 109(9): 937-941. <https://doi.org/10.2307/3454995>
- [15] Farhan, R.Z., Ebrahim, S.E. (2021). Preparing nanosilica particles from rice husk using precipitation method. *Baghdad Science Journal*, 18(3): 494-500. <https://doi.org/10.21123/bsj.2021.18.3.0494>
- [16] Ahmedzeki, N.S., Ali, S.M., Al-Karkhi, S.R. (2017). Synthesis and characterization of tri-composite activated carbon. *Iraqi Journal of Chemical and Petroleum Engineering*, 18(3): 49-58. <https://doi.org/10.31699/IJCPE.2017.3.4>
- [17] Yang, T., Lua, A.C. (2006). Textural and chemical properties of zinc chloride activated carbons prepared from pistachio-nut shells. *Materials Chemistry and Physics*, 100(2-3): 438-444. <https://doi.org/10.1016/j.matchemphys.2006.01.039>
- [18] Vijay, R., Tarika, K. (2019). Microbial production of polyhydroxyalkanoates (PHAs) using kitchen waste as an inexpensive carbon source. *Biosciences Biotechnology Research Asia*, 16(1): 155-166. <https://doi.org/10.13005/bbra/2733>
- [19] Bediako, J.K., Lin, S., Sarkar, A.K., Zhao, Y., et al. (2020). Evaluation of orange peel-derived activated carbons for treatment of dye-contaminated wastewater tailings. *Environmental Science and Pollution Research*, 27: 1053-1068. <https://doi.org/10.1007/s11356-019-07031-8>
- [20] Dhelipan, M., Arunchander, A., Sahu, A.K., Kalpana, D. (2017). Activated carbon from orange peels as supercapacitor electrode and catalyst support for oxygen reduction reaction in proton exchange membrane fuel cell. *Journal of Saudi Chemical Society*, 21(4): 487-494. <https://doi.org/10.1016/j.jscs.2016.12.003>
- [21] Cheng, P., Li, T., Yu, H., Zhi, L., Liu, Z., Lei, Z. (2016). Biomass-derived carbon fiber aerogel as a binder-free electrode for high-rate supercapacitors. *The Journal of Physical Chemistry C*, 120(4): 2079-2086. <https://doi.org/10.1021/acs.jpcc.5b11280>
- [22] Mehare, M.D., Deshmukh, A.D., Dhoble, S.J. (2021). Bio-waste lemon peel derived carbon-based electrode in perspective of supercapacitor. *Journal of Materials Science: Materials in Electronics*, 32(10): 14057-14071. <https://doi.org/10.1007/s10854-021-05985-5>
- [23] Barrett, E.P., Joyner, L.G., Halenda, P.P. (1951). The determination of pore volume and area distributions in porous substances. I. Computations from nitrogen isotherms. *Journal of the American Chemical Society*, 73(1): 373-380. <https://doi.org/10.1021/ja01145a126>
- [24] Dąbrowski, A. (2001). Adsorption—From theory to practice. *Advances in Colloid and Interface Science*, 93(1-3): 135-224. [https://doi.org/10.1016/S0001-8686\(00\)00082-8](https://doi.org/10.1016/S0001-8686(00)00082-8)
- [25] Li, Y., Li, Z., Shen, P.K. (2013). Simultaneous formation of ultrahigh surface area and three-dimensional hierarchical porous graphene-like networks for fast and highly stable supercapacitors. *Advanced Materials (Deerfield Beach, Fla.)*; 25(17): 2474-2480. <https://doi.org/10.1002/adma.201205332>
- [26] Wu, Z.S., Sun, Y., Tan, Y.Z., Yang, S., Feng, X., Müllen, K. (2012). Three-dimensional graphene-based macro- and mesoporous frameworks for high-performance electrochemical capacitive energy storage. *Journal of the American Chemical Society*, 134(48): 19532-19535. <https://doi.org/10.1021/ja308676h>
- [27] Bejar, A.K., Mihoubi, N.B., Kechaou, N. (2012). Moisture sorption isotherms—Experimental and mathematical investigations of orange (*Citrus sinensis*) peel and leaves. *Food Chemistry*, 132(4): 1728-1735. <https://doi.org/10.1016/j.foodchem.2011.06.059>
- [28] Mahmood, A.U., Greenman, J., Scragg, A.H. (1998). Orange and potato peel extracts: Analysis and use as *Bacillus* substrates for the production of extracellular enzymes in continuous culture. *Enzyme and microbial technology*, 22(2): 130-137. [https://doi.org/10.1016/S0141-0229\(97\)00150-6](https://doi.org/10.1016/S0141-0229(97)00150-6)
- [29] Kumar, M.A., Ravikumar, C.R., Murthy, H.A., Alam, M.W., et al. (2021). Fabrication of carbonized flakes epoxy electrode using lemon rind for supercapacitor applications. *Case Studies in Chemical and Environmental Engineering*, 3: 100090. <https://doi.org/10.1016/j.cscee.2021.100090>
- [30] Raghu Vamshi Krishna, B.V., Nageswara Rao, T., Murthy, H.A. (2023). Orange peel-derived activated carbon as an electrode material for supercapacitor application using nickel mesh. *Chemical Papers*, 77(9): 4953-4962. <https://doi.org/10.1007/s11696-023-02833-0>
- [31] Ruan, C., Ai, K., Lu, L. (2014). Biomass-derived carbon materials for high-performance supercapacitor electrodes. *RSC Advances*, 4(58): 30887-30895. <https://doi.org/10.1039/C4RA04470C>
- [32] Brunauer, S., Emmett, P.H., Teller, E. (1938). Adsorption of gases in multimolecular layers. *Journal of the American Chemical Society*, 60(2): 309-319. <https://doi.org/10.1021/ja01269a023>
- [33] Mishra, P., Singh, K., Dixit, U. (2021). Adsorption, kinetics and thermodynamics of phenol removal by ultrasound-assisted sulfuric acid-treated pea (*Pisum sativum*) shells. *Sustainable Chemistry and Pharmacy*, 22: 100491. <https://doi.org/10.1016/j.scp.2021.100491>
- [34] Alobaidi, D.S., Alwared, A.I. (2023). Role of immobilised Chlorophyta algae in form of calcium alginate beads for the removal of phenol: Isotherm, kinetic and thermodynamic study. *Heliyon*, 9(4): e14851.
- [35] Mhawesh, T.H., Abd Ali, Z.T. (2020). Reuse of brick waste as a cheap-sorbent for the removal of nickel ions from aqueous solutions. *Iraqi Journal of Chemical and Petroleum Engineering*, 21(2): 15-23. <https://doi.org/10.31699/IJCPE.2020.2.3>
- [36] Hussain, O.A., Hathout, A.S., Abdel-Mobdy, Y.E., Rashed, M.M., Rahim, E.A., Fouzy, A.S.M. (2023). Preparation and characterization of activated carbon from agricultural wastes and their ability to remove chlorpyrifos from water. *Toxicology Reports*, 10, 146-154. <https://doi.org/10.1016/j.toxrep.2023.01.011>
- [37] Abd AL-Hussain, Z.K., Abdul-Hameed, H.M. (2023). Removal of lead ions from wastewater by using a local adsorbent from charring tea wastes. *Iraqi Journal of Chemical and Petroleum Engineering*, 24(3): 93-102. <https://doi.org/10.31699/IJCPE.2023.3.9>

NOMENCLATURE

OP	Orange Peel
AC	Activated Carbon
gm	Gram
nm	Nano Material
N ₂	Nitrogen Gas
CO ₂	Carbon Dioxide Gas
V	Volume
°C	Celsius Degree
D	Size
K	Shape Factor
FTIR	Fourier Transform Infrared Spectroscopy
TEM	Transmission Electron Microscopy
SEM	Scanning Electron Microscopy

BET	Brunauer–Emmett–Teller (used for surface area analysis)
EDS	Energy Dispersive Spectroscopy
P/P ₀	Relative Pressure (used in BET analysis)
dP	Pore Diameter
VT	Total Pore Volume

Greek symbols

λ	0.154nm (X-ray wavelength)
β_{hkl}	Half-width of the diffraction band (FWHM)(radians)
ϑ_{hkl}	Bragg diffraction angle (peak position in radians)
μm	Micrometer